PROCEEDINGS OF SCIENCE

Unification of active galaxies from the perspective of X-ray polarimetry

A.V. Dorodnitsyn
Laboratory for High Energy Astrophysics, NASA Goddard Space Flight Center, Code 662, Greenbelt, MD, 20771, USA

T. Kallman
Laboratory for High Energy Astrophysics, NASA Goddard Space Flight Center, Code 662, Greenbelt, MD, 20771, USA

Active Galactic Nuclei (AGN), Seyfert galaxies and quasars, are powered by luminous accretion and often accompanied by winds which are powerful enough to affect the AGN mass budget, and whose observational appearance bears an imprint of processes which are happening within the central parsec around the black hole (BH). One example of such a wind is the partially ionized gas responsible for X-ray and UV absorption ('warm absorbers'). Here we show that such gas will have a distinct signature when viewed in polarized X-rays. Observations of such polarization can test models for the geometry of the flow, and the gas responsible for launching and collimating it. We present calculations which show that the polarization depends on the hydrodynamics of the flow, the quantum mechanics of resonance line scattering and the transfer of polarized X-ray light in the highly ionized moving gas. The results emphasize the three dimensional nature of the wind for modeling spectra. We show that the polarization in the 0.1-10 keV energy range is dominated by the effects of resonance lines. We predict a $5-25\%$ X-ray polarization signature of type-2 objects in this energy range. These results are general to flows which originate from a cold torus-like structure, located $\sim$ 1pc from the BH, which wraps the BH and is ultimately responsible for the apparent dichotomy between type 1 and type 2 AGNs. Such signals will be detectable by future dedicated X-ray polarimetry space missions, such as the NASA Gravity and Extreme Magnetism SMEX, GEMS [26]

25th Texas Symposium on Relativistic Astrophysics - TEXAS 2010
December 06-10, 2010
Heidelberg, Germany

PoS(Texas 2010)048

1. Introduction

Optical spectropolarimetry of Seyfert 2 galaxies was responsible for the revelation that both Seyfert 1 and Seyfert 2 AGNs are intrinsically the same objects, and that their apparent differences are due to the inclination from which they are viewed [1]. A paradigm of a cold ($T = 100 - 1000$K and several parsecs in diameter) molecular torus which is obscuring the broad line region in most low and intermediate luminosity AGNs, is supported by the polarized optical line spectra and in some cases by direct interferometric observations [12].

The obscuring torus may represent part of a flow originating at smaller [10] or larger [24] radii. Studies of the lines blueshifts combined with variability studies of warm absorber spectra [2, 22], suggest a location of the torus at the distance $\gtrsim$ 1pc from the BH.

First principal arguments [15, 16] support the idea that the torus is the source of an outflow which is evaporated by X-ray heating, and such gas is a plausible source of warm absorbers [17, 18].

The question of the origin of the warm absorber flow is intrinsically related to the problem of the vertical support of the torus against collapse. Infrared radiation pressure is a likely mechanism for such support [19], although magnetic fields could also contribute [20]. One may also expect large scale magnetic fields playing a role in producing hydromagnetic flows related to warm absorbers. Models based on self-similar solutions of the type developed by [4] were calculated by [9], [6], and [5]; warm absorber spectra in transmission from a different type of 2D self-similar solutions of the Grad-Shafranov equation were calculated by [11].

Warm absorber gas is heated and ionized by X-rays from the BH and in the low density limit such gas approaches the 'Compton temperature', $T_{IC} \sim 10^7$K, although multidimensional hydrodynamic simulations show that due to adiabatic losses the temperature may be smaller, $\sim 10^6$ K [7, 8]. It also follows that mass loss rates of $\dot{M} = 0.1 - 1\,M_\odot/\mathrm{yr}$ and velocities of $100 - 1000\,\mathrm{km\,s^{-1}}$ are attainable, and that these properties match those of X-ray warm absorbers.

Free electrons in the wind scatter radiation from the accretion disk and broad line region towards the observer giving rise to the polarized optical and UV [1] spectrum in Seyfert 2 objects. Highly ionized ions from this same mirror gas create rich X-ray spectra of warm absorbers at inclinations appropriate for Seyfert 1 objects. These correspond to photoionized plasma with numerous absorption and emission lines from highly ionized ions of Fe, Si, S, O, and Ne in the 0.1 - 10 keV energy range. These are detected by the *Chandra* and *XMM − Newton* satellites, in addition to features from many of the same ions in the UV seen by e.g. *HST*. Such spectra occur in a large fraction of low redshift AGNs which are bright enough to allow detection [25, 21]. These lines occur in absorption in Seyfert 1 galaxies, and in reflection spectra in Seyfert 2 galaxies [14], corresponding to differing views of the flow and torus.

X-ray polarimetry promises a new opportunity to study AGN winds through their X-ray reflection and thus to test AGN unification models. Here we report the results of self-consistent modeling of the X-ray polarization signature produced by a warm absorber flow. We choose a torus model with initial mass $M_{\rm tor} = 9.3 \cdot 10^5\,M_\odot$, so the maximum Compton optical depth of the torus interior, $\tau_{\rm max} = 40$, is high enough to ensure capture of essentially all X-rays incident on the torus inner surface. We calculate the evolution of such gas and the fate of the torus, using the techniques described in [7, 8], which includes the dynamics and the effects of photoionization and photon heating on the thermal and opacity properties in the gas [13].

Gas evaporated by X-ray heating is confined by the torus funnel. Our calculations suggest that to some extent, the throat of the torus acts similar to a de Laval nozzle in a rocket engine, simultaneously providing the flow with the fuel through evaporation of the material of the confining walls. This helps to convert the internal energy of the heated gas to bulk kinetic energy of the outflow. Some of the X-ray heated gas is close enough to the black hole to capture significant radiation flux and contributes to the polarization signature. This is enhanced by gas which fails to escape from the potential well, forming a returning current. The opening of the torus funnel is affected by the hydrodynamics of evaporation and determines the fraction of AGN in which warm absorber spectra can be observed [8].

2. Results

A notable feature of most warm absorber spectra is the fact few of the lines appear truly black in their cores. While this could be due to finite resolution or finite column of the gas, in our simulations this is because of scattering into the line core. Such scattering typically occurs at angles close to 90^o, and so the residual flux in the lines is highly polarized. This is similar to the polarization of the (rest frame) UV lines observed from broad absorption line quasars [23]. Figure 1 shows spectra and the corresponding polarization fraction, P at inclination $\theta = 50^\circ$ after the wind simulation has evolved through four dynamical times (the dynamical time is given by: $t_0 = 1.5 \times 10^4\, r_{\rm pc}\, (M_{\rm BH}/M^6_\odot)^{-1/2}\,({\rm yr})$, where $M_{\rm BH}/M^6_\odot$ is the BH mass in units of $10^6 M_\odot$ and $r_{\rm pc}$ is the radius of the torus in pc) Each synthetic spectrum is convolved with a Gaussian with width and centroid related by $\sigma_E = 10^{-3}E$. In the 0.1-10 keV range, the most prominent feature of the spectrum is an absorption trough (Figure 1, upper panel) and a corresponding maximum in polarization at $\sim 14.9-17.2,\ (0.72-0.83$ keV). This is due to H-, and He-like oxygen and moderately ionized iron, Fe XVII $-$ Fe XIV. The polarization maximum has $P_{\rm max} = 10\%$, and polarization at FWHM=0.05 keV about 2%. This is produced at a distance $\simeq$2.1 pc from the BH, where the radial column density rises from $N_{\rm col} = 1.5 \cdot 10^{22}$ to $N_{\rm col} = 3.8 \cdot 10^{22}$, and the ionization parameter, ξ [27] drops from $6.4 \cdot 10^3$ to $500-10$ within a region $2.8-4.4$ pc. This results in an ideal situation for scattering in the flow, since further away the plasma is again over-ionized: $\xi \sim 10^4$. Polarization of lines in the 0.1-2 keV band is generally $\leq$1%, but for the strongest lines the polarization can reach 2 – 3% in the O VIII Lα and Ne IX He α lines; and $\simeq$10% in the case of the features at $\sim$ 0.75 keV.

At high inclinations, $\theta \gtrsim 60^\circ$, most lines appear in emission, and the continuum flux is $\sim 10^{-2}$ of that at low inclinations. Figure 2 shows the spectrum and corresponding polarization fraction, P at inclination $\theta = 70^\circ$. One of the insights provided by multi-dimensional transfer calculations is the importance of blending of multiple lines, i.e. when several lines collectively appear as a single strong feature. Blending of multiple lines from Fe XXV and Fe XXVI forms such a spectral feature at $E_0 \sim 6.5$ keV, at the inclination in Figure 2, resembling a P-Cygni line. However, this shape is not due to the effect of the moving wind, rather it is an interplay between geometric effects and ionization balance. That is, due to the attenuation of the continuum at high inclinations, when the continuum intensity in the line emitting region falls below a threshold, $I_{\rm c} \lesssim S_{\rm l}(1-e^{\tau})$, where $S_{\rm l}$ is the source function and $\tau_{\rm l}$ is the optical depth, then the ensemble of lines corresponding to lower ionized gas pops up above the continuum, while the more highly ionized gas is still seen

in absorption. Other examples of such features occur at lower inclinations, such as at $\theta \simeq 45^\circ$, corresponding to the O VII edge at 16.8 (739 eV), together with lines from the L shell of Fe.

Figure 3 shows the distribution of polarization fraction versus inclination angle. We plot the maximum polarization, $P_{\rm max}$ (P convolved with a Gaussian with $\sigma_E = (15)^{-1}E$), and the flux mean $< P >_{\rm F}$ in the 0.1-2 and 2-10 keV bands. This shows that the maximum polarization is $< P >_{\rm max} \simeq 15-20\%$ over a wide range of angles. The various peaks and troughs in this plot are reflections of the density structure in the flow, including wedges of gas which are stripped off the torus. The flux mean polarization has a maximum near $\theta = 67^\circ$, where $< P >_{\rm F} (0.1-2)\,{\rm keV} \lesssim 10\%$ and $< P >_{\rm F} (2-10)\,{\rm keV} \lesssim 2\%$. At $\theta \gtrsim 75^\circ$ the flux mean polarization in the 0.1-10 keV range is $< P >_{\rm F} \lesssim 20\%$ and the maximum is $P_{\rm max} \simeq 70\%$. At such inclinations the torus is Compton thick along the line of sight and the continuum flux is very low, $\leq 1\%$ of the unattenuated value.

Scattering by free electrons from optically thin plasma can produce a continuum polarization fraction which is comparable to that in the lines [3]. Optically thin, single scattering approximation provides an upper limit for the polarization.

This approach takes into account the geometry of the problem together with optical depth effects and predicts both the polarized flux and the fractional polarization is less than those produced by lines. This is shown as the labeled curve in Figure 3). At those viewing angles where the Thomson continuum has significant polarization, the flux is $\sim (10^{-3}-10^{-4})F_{\rm c}$, where $F_{\rm c}$ is the flux of the core.

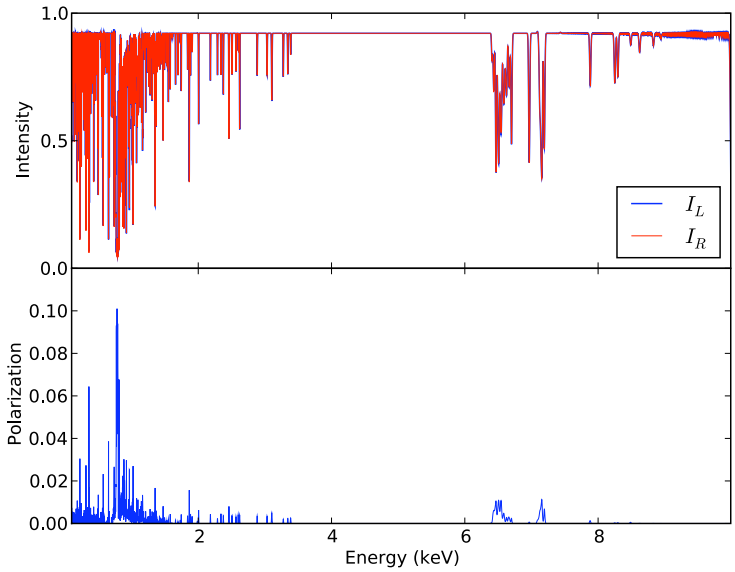

Figure 1: Warm absorber spectra viewed at inclination 50° in two orthogonal linear polarization modes, $I_{\rm L}$,$I_{\rm R}$ (up). Polarization fraction, P (bottom).

Our results show that models in which the obscuring torus is the source of an X-ray excited flow generate potentially observable polarization signatures due to significant scattering of X-rays by atomic features in the flow. Thomson electron scattering continuum at $\theta \lesssim 60^\circ$ has polarization $< 1\%$; it is increasing to a maximum of 17% at $\theta \simeq 80^\circ$, and then decreases at larger θ. Polar-

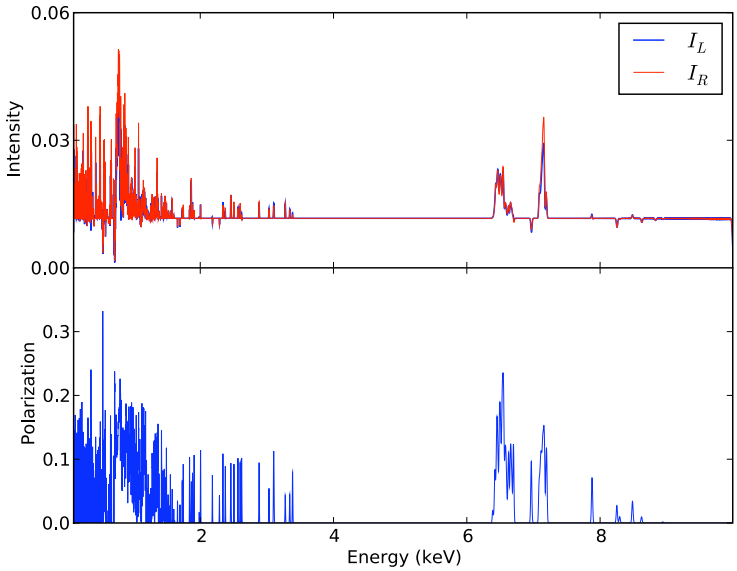

Figure 2: Same model as in Figure 2 but at inclination 70°.

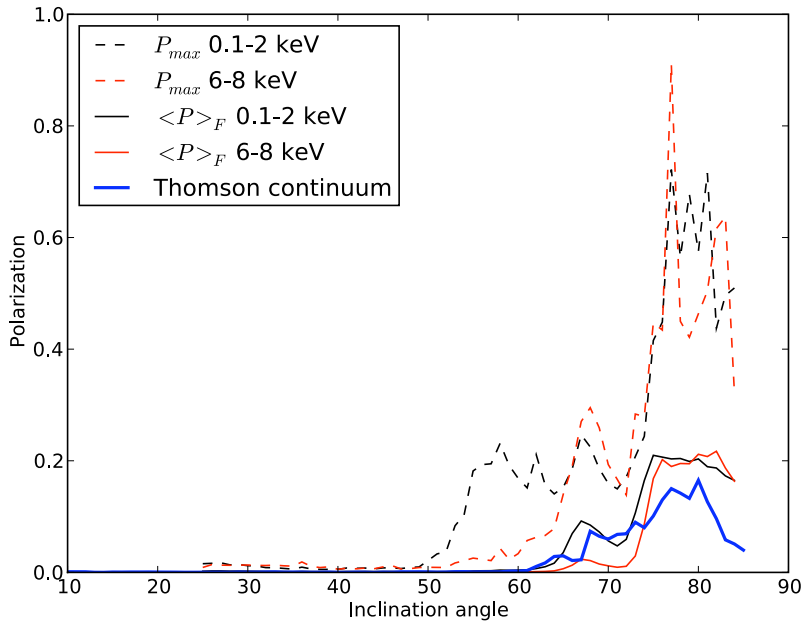

Figure 3: Distribution of the polarization fraction with inclination angle. Curves: dashed: maximum polarization fraction within the energy range; solid: thin: flux mean polarization fraction within the energy range; thick: Thomson scattering continuum

ization from lines is greater and has the following properties: at very low inclination, $\theta \lesssim 45^\circ$, corresponding to prototypical Seyfert 1 galaxies, the linear polarization fraction is negligible averaged over the spectrum, but most absorption lines have some residual, highly polarized flux; the maximum polarization fraction in strong lines is $1-10\%$. At higher inclinations, $45^\circ \lesssim \theta \lesssim 75^\circ$ in the 0.1-2 keV range the mean polarization is 10%, and the maximum polarization is 20-30%; in the 6-8 keV range the mean polarization is 2-10%, and the maximum polarization 20-30%. At still higher inclinations $\theta \gtrsim 70-80^\circ$ our models are very Compton thick. Scattering in X-ray lines above the torus funnel produces very strongly polarized flux with mean polarization fraction more than 20% and maximum polarization 60-70%. Although these predictions are specific to our dynamical calculations, the general behavior will hold for any scenario involving an outflow which is shadowed by a torus with aspect ratio near unity. Observations which fail to show such high polarization would call into question current ideas about the torus location, shape and thickness.

References

[1] Antonucci, R.R.J., Miller, J.S. 1985, *ApJ*, 297, 621

[2] Behar, E., Rasmussen, A.P., Blustin, A.J., et al. 2003, *ApJ*, 598, 232

[3] Bianchi, S., Matt, G., Tamborra, F., Chiaberge, M., Guainazzi, M., Marinucci, A. 2009, astro-ph:0905.4845

[4] Blandford, R. D., Payne, D. G. 1982 *MNRAS*, 199, 883

[5] Bottorff, M., Korista, K.T., Shlosman, I. *ApJ* 537, 134

[6] Bottorff, M., Korista, K.T., Shlosman, I. & Blandford, R.1997, *ApJ* 479, 200

[7] Dorodnitsyn, A., Kallman, T., Proga, D. 2008, *ApJL* 657, 5

[8] Dorodnitsyn, A., Kallman, T., Proga, D. 2008, *ApJ*, 687, 97

[9] Emmering, R.T., Blandford, R. & Shlosman, I. 1991, *ApJ*, , L101

[10] Elitzur, M., & Shlosman, I. 2006, Ap.J.L., 648, L101

[11] Fukumura, K., Kazanas, D., Contopoulos, I. 2009 astro-ph:0910.3001v1

[12] Jaffe et al. 2004, Nature, 429, 47

[13] Kallman, T., Bautista, M. 2001, ApJS, 133, 221

[14] Kinkhabwala, A., Sako, M., Behar, E., Kahn, S.M., Paerels, F., Brinkman, A.C., Kaastra, J.S., Ming Feng Gu, Liedahl, D.A. 2002, *ApJ*, 575, 732

[15] Krolik, J.H., Begelman, M.C. 1986, *ApJ*, 308, L55

[16] Krolik, J.H., Begelman, M.C. 1988, *ApJ*, 329, 702

[17] Krolik, J.H., Kriss, G.A. 1995, *ApJ*, 447, 512

[18] Krolik, J.H., Kriss, G.A. 2001, *ApJ*, 561, 684

[19] Krolik, J.H. 2007, *ApJ*, 661, 52

[20] Lovelace, R., Romanova, M., Biermann, P. 1998, *A&A*, 338, 856

[21] McKernan, B., Yaqoob, T., Reynolds, C. S. 2007 *MNRAS*, 379, 1359

[22] Netzer et al. 2003, *ApJ*, 599, 933N

[23] Ogle et al. 1999, *ApJS*, 125, 1

[24] Proga, D. 2007,*ApJ*,661,693

[25] Reynolds, C.S. 1997, *MNRAS*, 286, 513

[26] Gravity and Extreme Magnetism SMEX (GEMS), 37th COSPAR Scientific Assembly, 2008

[27] Tarter, C.B., Tucker, W., Salpeter, E.E. 1969, *ApJ*, 156, 943